Supporting Information for

Free-Standing 3D Nitrogen-Carbon Anchored Cu Nanorod Arrays: *In-Situ* Derivation from Metal-Organic Framework and Strategy to Stabilize Lithium Metal Anode

Dongming Yin,[a] Gang Huang,[a,c] Shaohua Wang,[a, b] Dongxia Yuan,[a, b] Xuxu Wang,[a, b] Qian Li,[a, b] Qujiang Sun,[a] Hongjin Xue,[a, b] Limin Wang[a, b] and Jun Ming*[a]*

[a] State Key Laboratory of Rare Earth Resource Utilization, Changchun Institute of Applied Chemistry, Chinese Academy of Sciences Changchun, 130022, P. R. China;

[b] University of Science and Technology of China, Heifei, 230026, P. R. China;

[c] WPI Advanced Institute for Materials Research, Tohoku University, Sendai 980-8577, Japan.

* To whom correspondence should be addressed: ghuang@ciac.ac.cn; jun.ming@ciac.ac.cn.

Keywords: Lithium metal anode, metal-organic framework, plating/stripping behavior, dendrite-free, nitrogen-carbon anchored copper

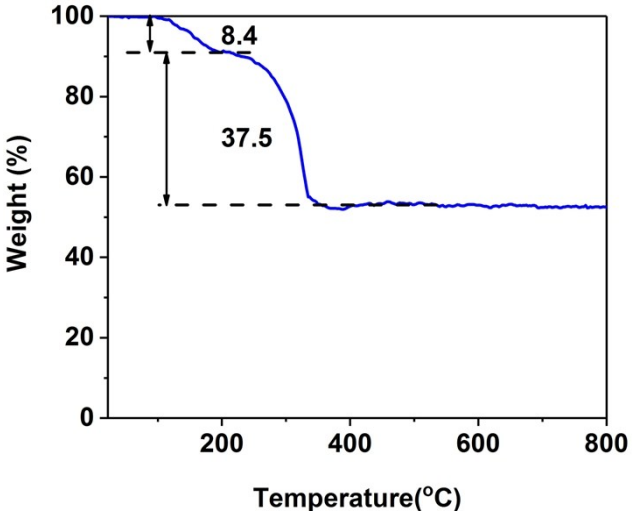

Figure S1. TG curve of Cu-MOF.

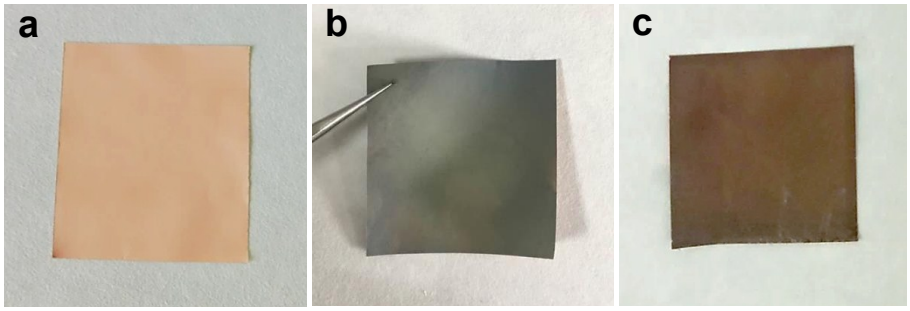

Figure S2. Digital photos of (a) Cu foil, (b) Cu-MOF and (c) NC/Cu.

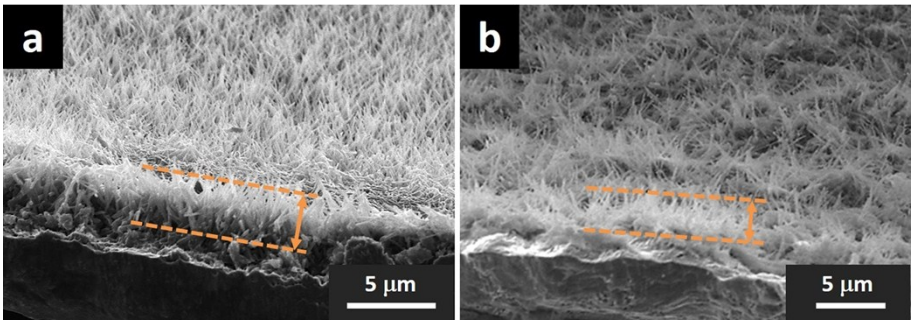

Figure S3. Cross-sectional SEM images of (a) Cu-MOF and (b) NC/Cu.

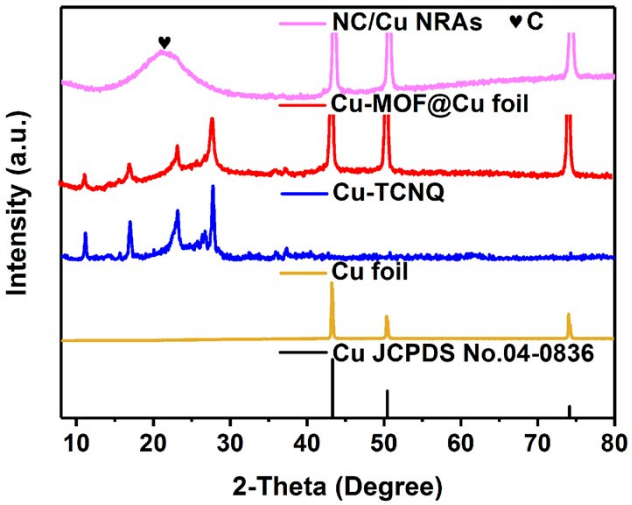

Figure S4. XRD patterns of Cu foil, Cu-TCNQ, Cu-MOF@Cu foil and NC/Cu.

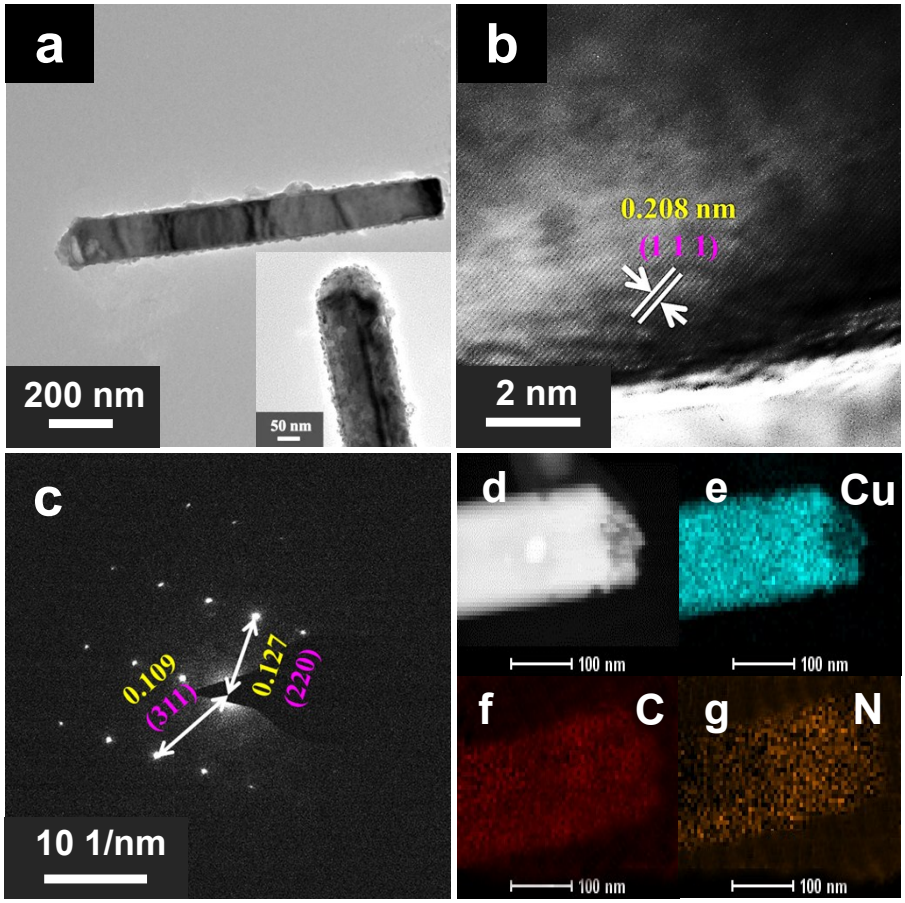

Figure S5. (a) TEM image, (b) HRTEM image, (c) SAED pattern, (d) HAADF-STEM image and (e-g) element mapping of NC/Cu.

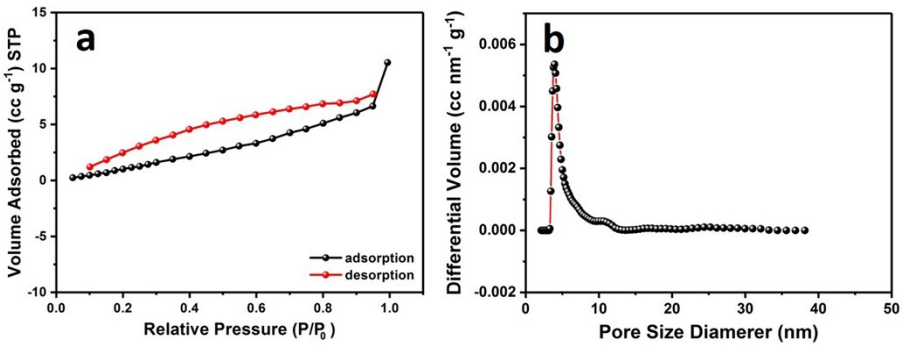

Figure S6. (a) N_2 adsorption-desorption isotherms and (b) pore size distribution curves of NC/Cu current collector.

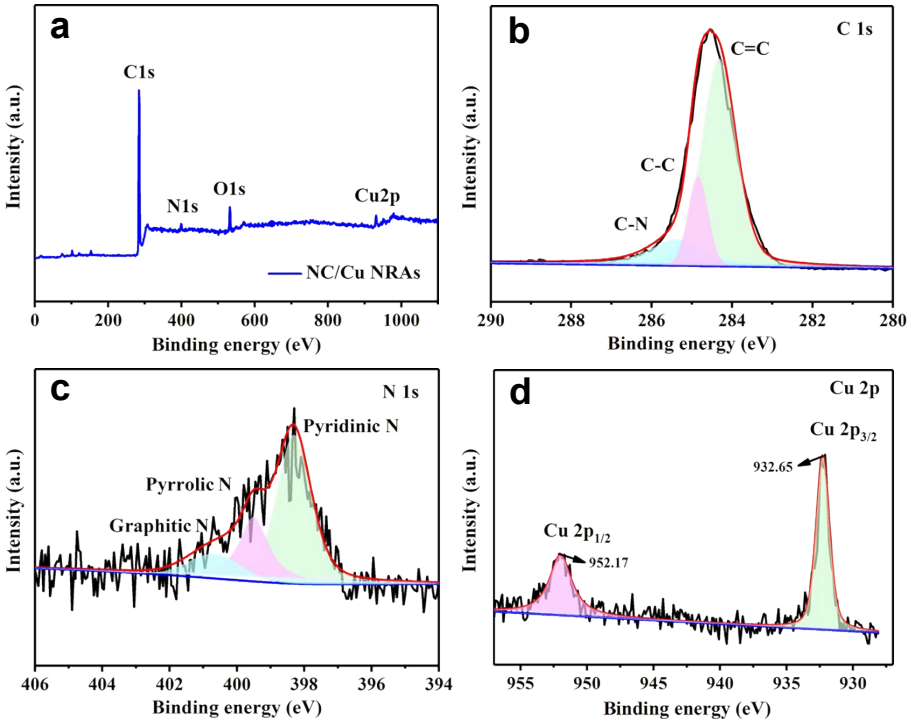

Figure S7. XPS spectra of (a) NC-Cu, (b) C 1s, (c) N 1s, and (d) Cu 2p. Note that the presence of O in (a) may result from the absorption of water molecules and oxygen in air.

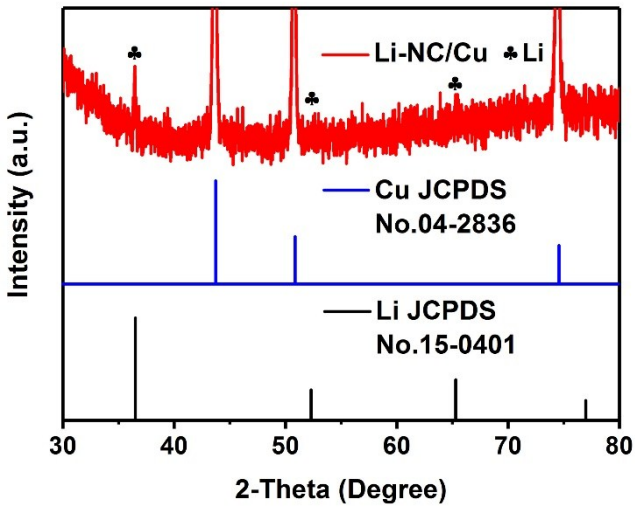

Figure S8. XRD pattern of NC/Cu electrode after lithium deposition.

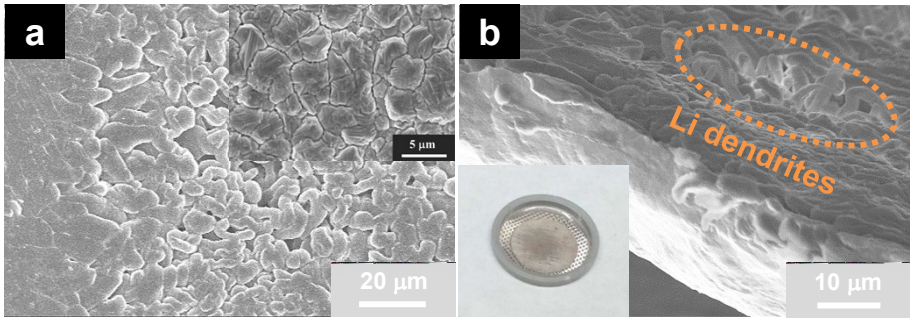

Figure S9. (a) Top view and (b) cross-sectional SEM images of lithium on Li-Cu electrode. Inset in (a) and (b) are the SEM image of Cu foil and the digital photo of Li-Cu electrode.

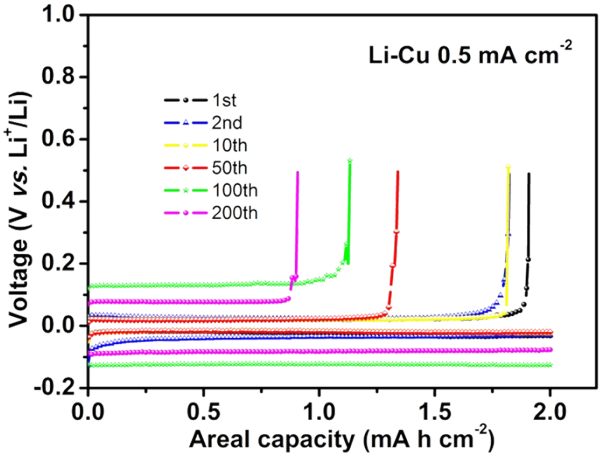

Figure S10. Voltage *vs.* capacity profiles of Li stripping/plating on Cu current collector at different cycles with a current density of 0.5 mA cm^{-2} for the areal capacity of 2 mAh cm^{-2}.

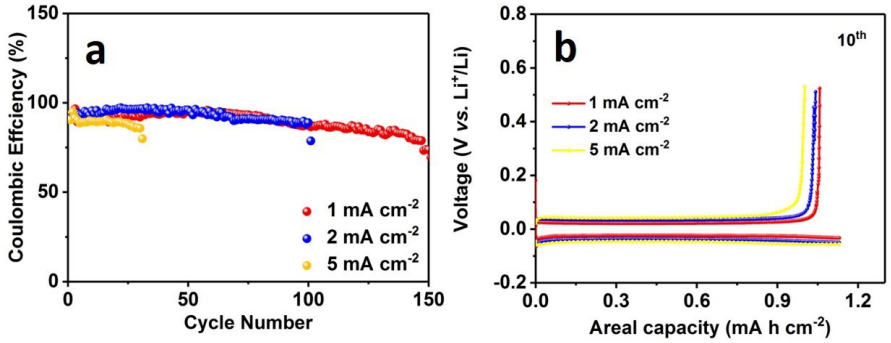

Figure S11. (a) Coulombic efficiencies of the cells using NC/Cu current collectors at 1, 2 and 5 mA cm^{-2}. (b) The 10^{th} voltage *vs.* capacity profiles of Li stripping/plating on NC/Cu current collectors with a specific capacity of 1 mAh cm^{-2} and current densities of 1, 2 and 5 mA cm^{-2}.

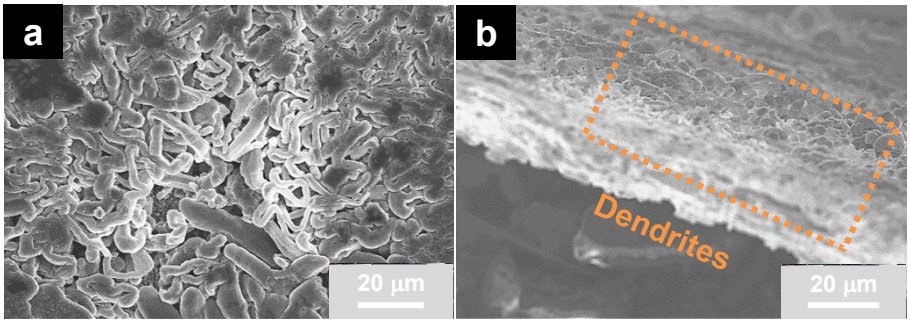

Figure S12. (a) Top view and (b) cross-sectional SEM images of Cu foil current collector after lithium deposition at the 50^{th} cycle.

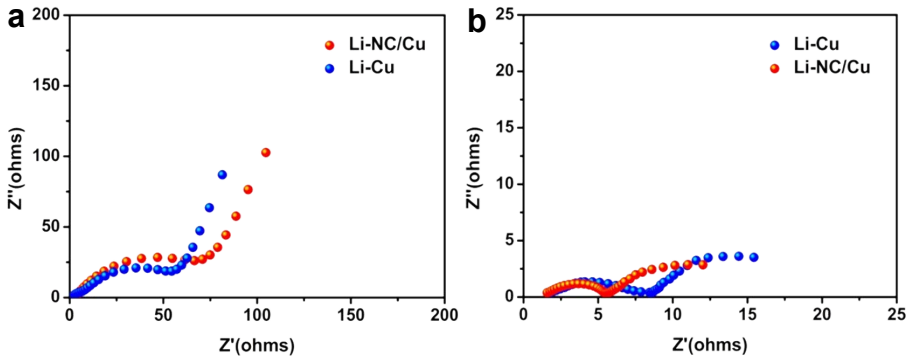

Figure S13. Comparative Nyquist plots of Li stripping/plating on NC/Cu and Cu foil current collectors (a) before cycle, (b) after the 50^{th} cycles at 0.5 mA cm^{-2} with the capacity of 2 mAh cm^{-2}.

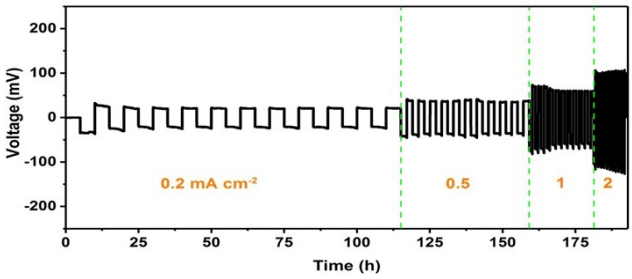

Figure S14. The voltage *vs.* time profiles of the Li-NC/Cu symmetric cell at different current densities.

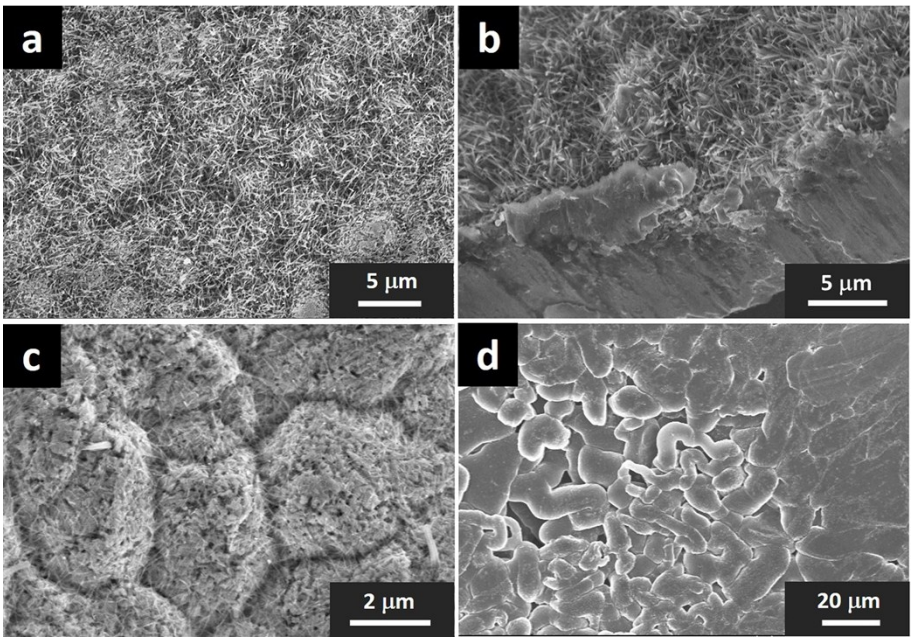

Figure S15. SEM images of (a) Cu foil at TCNQ acetonitrile solution for 12 h, (b) the corresponding cross-sectional image, (c) NC/Cu-12 and (d) NC/Cu-12 deposited with 2 mAh cm^{-2} of Li.

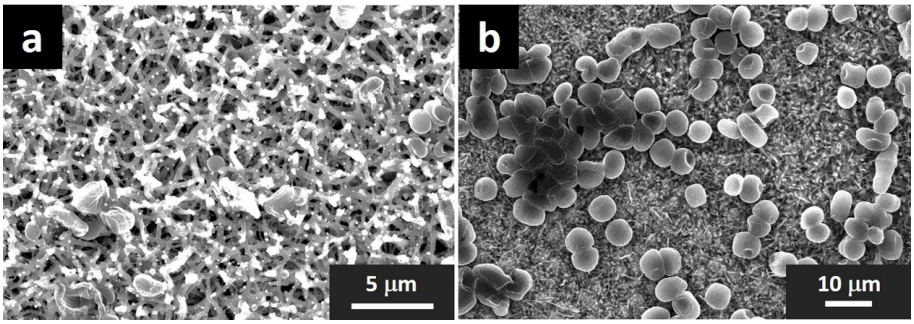

Figure S16. SEM images of NC/Cu deposited with (a) 0.2 and (b) 0.5 mAh cm^{-2} of Li.

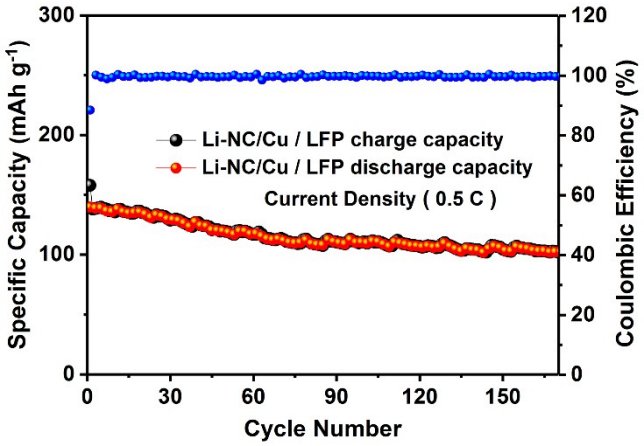

Figure S17. Cycling performance of Li-NC/Cu‖LFP full cell at 0.5 C.

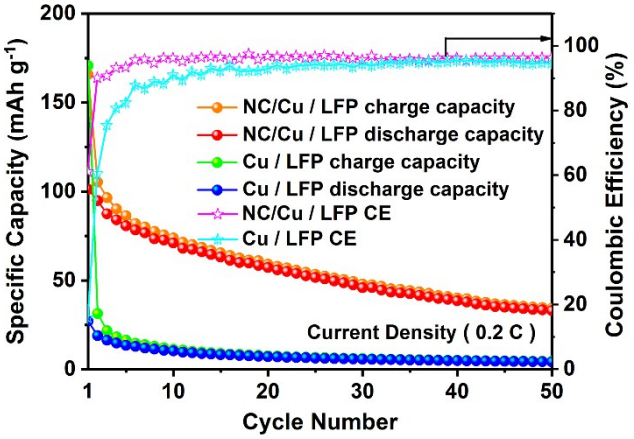

Figure S18. The discharge-charge capacities and corresponding CEs of the NC/Cu ‖ LFP and Cu foil ‖ LFP cells at 0.2 C.